Clays and Clay Minerals (2024), **72**, e28, 1–9
doi:10.1017/cmn.2024.31

Original Paper

Mechanical properties of pristine smectite clay minerals and clay–polymer hybrids studied by density functional theory

Sanam Bashir[1], Daniel Tunega[2] and Eva Scholtzová[1]

[1]Institute of Inorganic Chemistry, Slovak Academy of Sciences, Dúbravská cesta 9, 845 36 Bratislava, Slovakia and [2]Institute of Soil Research, Department of Forest and Soil Sciences, University of Natural Resources and Life Sciences, Peter-Jordan-Strasse 82b, A-1190 Wien, Austria

Abstract

Recent years have seen significant interest in the mechanical properties of clay–polymer hybrids due to their suitability for possible application as sustainable materials in green chemistry. The objective of the present study was to investigate the mechanical properties of clay–polymer hybrids and their corresponding pristine smectite clay minerals. The density functional theory (DFT) method, employing the D3 scheme for corrections of dispersion interactions, was used to calculate elastic constants (C_{ij}) of models of pristine smectites, particularly montmorillonite, beidellite, saponite, and hectorite, and their hybrids built on the polymer poly(2-methyl-2-oxazoline), PMeOx. Following that, the elastic moduli, encompassing the bulk modulus (K_{VRH}), shear modulus (G_{VRH}), Young's modulus (E_{VRH}), and Poisson's ratio (v), were calculated. The results revealed a reduction in elastic constants and elastic moduli following the intercalation of smectite clay minerals with the PMeOx polymer. The findings highlighted a distinctive ranking of mechanical properties among pristine smectite clay minerals and clay–polymer hybrids, with hectorite and its hybrid (Htr-PMeOx) demonstrating better performance compared with saponite, montmorillonite, and beidellite and their respective hybrids.

Keywords: clay–polymer hybrids; density functional theory; elastic constants; poly(2-methyl-2-oxazoline); smectites

(Received: 26 February 2024; revised: 30 June 2024; accepted: 19 August 2024)

Introduction

Research on clay–polymer nanocomposites (CPNs) has advanced over the last decade, focusing on improving mechanical and physical-chemical properties, creating sustainable materials, and exploring various applications such as wastewater treatment, food packaging, and biomedical applications. CPNs offer a promising future in creating strong, biodegradable, and multifunctional materials (Mukhopadhyay et al., 2020; Niu et al., 2021; Cheikh et al., 2022; Das et al., 2022; Masood et al., 2022).

Clay minerals of the smectite family typically have a large surface area and a large cation exchange capacity, which makes them useful as adsorbents, catalysts, and in various environmental remediation applications (Brigatti et al., 2006). Based on the ability to exchange interlayer cations, the CPNs are formed by intercalating polymers into the interlayer space of smectites. Other benefits of employing smectites as a viable filler for CPNs are affordability, eco-friendliness, and abundance. Contrary to traditional micro-fillers, smectites can dramatically improve the characteristics of a polymer matrix when used as a nanofiller (5 wt.%). Because smectites and polymers have a large interfacial area, stress is transferred from polymers to smectites, improving the mechanical strength of CPNs (Zare et al., 2017; Adak et al., 2018; Monjarás-Ávila et al., 2020). A significant amount of experimental research was carried out to prove that CPNs have excellent mechanical properties. For example, CPN based on sodium montmorillonite (Na-Mnt) could be employed in dental applications because of their improved mechanical and chemical properties (Monjarás-Ávila et al., 2020). Enhancements in tensile strength, flexural strength, and moduli were observed by the introduction of a clay mineral into an epoxy/glass nanocomposite (Karippal et al., 2011). Intercalation of a polymer into the interlayer space of clay minerals enhanced the mechanical properties of the pristine polymer. For example, the tensile strength measured for polypropylene/organic montmorillonite nanocomposite was 49.6 MPa, significantly more than the tensile strength of pristine polypropylene (41.3 MPa) (Zhang et al., 2017). The Young's modulus of pristine poly(butylene terephthalate) increased from an initial value of 2.5±0.1 GPa to 2.6±0.1 GPa and further to 2.7±0.1 GPa upon the addition of 4.9 wt.% and 3.7 wt.% of modified natural Brazilian smectite (Colombo et al., 2023).

Using organo-modified layered silicates is common practice to enhance the compatibility between the filler and matrix, as most polymers exhibit organophilic properties. One often-widely employed technique for modification is the incorporation of surfactants that are readily obtainable on the market into the interlayer space through cation exchange reactions. Montmorillonite modified with benzothiazolium surfactant

Corresponding author: Eva Scholtzová; Email: eva.scholtzova@savba.sk
Cite this article: Bashir S., Tunega D., & Scholtzová E. (2024). Mechanical properties of pristine smectite clay minerals and clay–polymer hybrids studied by density functional theory. *Clays and Clay Minerals* **72**, e28, 1–9. https://doi.org/10.1017/cmn.2024.31

improved the mechanical and thermal properties of polyamide 6 nanocomposites (Mekhzoum et al., 2020). The tensile strength and Young's modulus of pristine polyvinyl chloride (PVC) were 1.58 MPa and 0.881 MPa, respectively. After the addition of a cationic surfactant, cetylpyridinium chloride – CPC, to the montmorillonite clay, the Young's modulus of the resultant organomontmorillonite (O-Mnt) and organobentonite (O-Bent) increased by a factor of 1.8 and 1.4, respectively. Increase in the tensile strength of PVC was observed by factors of 1.7 (for OMnt), 1.8 (for OBent), and 1.3 (for OVt) after reinforcing the modified clay minerals (Kumari et al., 2023). To create CPN materials for engineering purposes, understanding the fundamental attributes of pristine clay minerals is essential. Clay minerals have nanoscale sizes and are strongly anisotropic. Thus it is challenging to assess mechanical properties directly by experimental means, e.g. by utilizing Brillouin spectroscopy (Scholtzová et al., 2015). This also generates interest in utilizing molecular modeling to determine these properties (Zheng and Zaoui, 2018). Attempts to perform first-principles calculation to model elastic constants began when the density functional theory (DFT) approach was used to compute elastic constants and bulk modulus of kaolinite, a non-expanding clay with minimal water adsorption capacity (Sato et al., 2005). Several studies followed this approach; for example, DFT methods and molecular dynamics were employed for assessing elastic constants of modified kaolinite and smectite clay minerals (Militzer et al., 2011; Ebrahimi et al., 2012; Scholtzová and Tunega, 2020; Zhao et al., 2021). These findings primarily used the theoretical molecular techniques at the nanoscale to discover the elastic properties of clay minerals. The increased interest in theoretical approaches is mainly because they can offer more detailed and complete predictions, which experimental methods often need help to provide. Similarly, the intricacy of chemical constituents at the nanometer scale, coupled with challenges in accurately managing the dispersion of nanofillers, has posed difficulties for experimental characterization methods to offer comprehensive insights into the mechanical reinforcement mechanism in CPN materials. Hence, experiments alone may not be able to determine accurately specific microscopic characteristics of CPNs, including the structure, mobility, and mechanical properties of the interlayer polymer. Based on this, the computational methods have proven to be a powerful tool in investigating various physical/chemical properties of polymer nanocomposites (Sharma and Devi, 2022). A combined application of DFT and molecular dynamics techniques was used to explore the function of montmorillonite-poly(lactic-co-glycolic acid) composites in facilitating the targeted delivery of phytochemicals, specifically curcumin (Karataş et al., 2017). Likewise, experimental methods and DFT calculations were used to study the interactions of carbon nanotubes and Mnt on the epoxy surface and determine their mechanical and thermal properties. When employed as an inorganic filler, Mnt has been shown to enhance conductivity and mechanical characteristics in solid polymer electrolytes (SPEs) (Khostavan et al., 2019). In the context of lithium metal batteries, the mechanism behind the ionic conductivity of Mnt-SPEs composites was elucidated through DFT, leading to impressive conductivity in lithium solid batteries (Wang et al., 2021). In another study, Na-Mnt enhanced the development of effective flocculants for wastewater treatment by incorporating the cationic polymer into the kaolinite and montmorillonite interlayer surface to study flocculation and sedimentation (Zhang et al., 2022; Wang et al., 2023).

Interest in a class of poly(2-alkyl-2-oxazoline) polymers (POx) has increased dramatically over the past two decades, for example in biological applications. The POxs are increasing in popularity as a possible replacement for polyethylene glycol, which is unfavorable due to its toxicity and instability (Trachsel et al., 2021). POxs are non-toxic and biocompatible and, because of this, can be used in various industrial applications such as biomedical and drug delivery (Platen et al., 2015; Glassner et al., 2018;). The interaction between poly(2-ethyl-2-oxazoline) (PetOx) and Mnt was studied and compared with pristine PetOx; clay–polymer nanocomposites (PetOx-Mnt) demonstrated improved heat stability (Ozkose et al., 2017). Only a few studies exist on how other clay minerals interact with POxs. Le Coeur et al. (2021) reported the interaction of PMeOx-laponite and the poly(ethylene oxide)-Laponite system. It was observed that the storage modulus (G′) behavior in PMeOx-based laponite hydrogels differs from PEO-based hydrogels, showcasing a unique strengthening mechanism due to increased PMeOx affinity for clay surfaces, reducing inhomogeneities and introducing steric repulsions. Using both experimental and theoretical research, the structural stability of Na-Mnt with polyethyleneimine (PEI) and PMeOx was investigated recently. Both composite models showed good stability, with the stability of Mnt-PMeOx slightly greater than that of PEI-Mnt (Madejová et al., 2023).

The present study aimed to conduct a comprehensive analysis of the mechanical properties of pristine smectite clay minerals and respective clay–polymer hybrids with PMeOx. The first section of the paper focused on the theoretical exploration of the structural stability and mechanical properties of smectite clay minerals, i.e. Mnt, beidellite (Bei), saponite (Sap), and hectorite (Htr). Knowledge of the mechanical properties of single minerals is very useful in the study of aggregates consisting of different types of minerals. Minerals with greater stiffness or strength will bear more load and contribute more to the overall strength of the aggregate. Weaker minerals may act as stress concentrators or preferential sites for crack initiation, affecting the overall failure mode of the aggregate (Sun et al., 2017). The second part of the manuscript analyzed the structural stability and mechanical properties of respective clay–polymer hybrids, specifically Mnt-PMeOx, Bei-PMeOx, Sap-PMeOx, and Htr-PMeOx. Their structural characteristics, elastic constants (C_{ij}), and other mechanical properties (employing the Voigt–Reuss–Hill average, VRH) (Hill, 1952) were determined through DFT calculations. The objective of the present study was to compare systematically, for the first time, the impact of four different typical smectites on the mechanical properties of the corresponding clay–polymer hybrids. Understanding the mechanical properties of smectite clay minerals and their respective clay–polymer hybrids should hold the potential for future use in environmental and industrial applications.

Computational details

Computational method

All calculations were conducted using the Vienna *Ab Initio* Simulation Package (VASP) (Kresse and Furthmüller, 1996). The exchange-correlation energy was described at the generalized gradient approximation (GGA) level using the Perdew-Burke-Ernzerhof (PEW) functional (Perdew et al., 1996). The solution

https://doi.org/10.1017/cmn.2024.31 Published online by Cambridge University Press

of the Kohn–Sham equations was executed using projector-augmented-wave (PAW) potentials (Blöchl, 1994) within a plane-wave basis set employing a kinetic energy cut-off of 600 eV, as the calculations of elastic properties require very precisely relaxed atomic positions and a highly converged absolute energy and stress tensor. Due to the large dimensions of the computational cells, sampling of the Brillouin zone was limited to the Γ-point. The optimization was performed with convergence criteria of 10^{-6} eV per atom for total energy changes and 0.015 eV Å^{-1} for residual forces on all atoms. No symmetry restrictions were applied during any relaxation procedure. All atomic positions and unit-cell parameters were relaxed. Cartesian axes were parallel to respective lattice vectors (x/a, y/b, z/c). Owing to weak interactions among the layers and intercalated species, DFT calculations were performed involving the D3 scheme for corrections of dispersion interactions (Grimme et al., 2010). For the determination of elastic constants (C_{ij}), a stress–strain approach (Nielsen and Martin, 1983) was employed as implemented in the VASP code. The elastic tensor was determined by performing finite distortions of the lattice and deriving the elastic constants from the stress–strain relationship. The deformations of the 0.015 Å size were done in positive and negative directions, and the strain tensor was calculated from the negative derivation of the energy with respect to the stress. This type of numerical calculation is sensitive to the parameters used, which can result in an error in the calculations. However, as the same set-up of parameters was used for all calculations, a potential error should be the same for all models, so the comparison of mechanical parameters of smectites is correct. Subsequently, the bulk (B), shear (G), and Young's (E) moduli were calculated from the derived C_{ij} values using the VHR average method (Carrier et al., 2014; Hill, 1952).

Computational model

The clay minerals such as montmorillonite, beidellite, saponite, and hectorite are classified within the smectite family of 2:1 clay minerals. A 2:1 clay mineral layer consists of an octahedral sheet sandwiched between two tetrahedral sheets. The structural diversity observed in smectite clay minerals stems from isomorphic substitutions occurring in the central atoms of either the tetrahedral or octahedral sheet. The octahedral sheet may be predominantly occupied by either trivalent cations, as seen in dioctahedral smectites like Mnt and Bei, or by divalent cations, as observed in trioctahedral smectites such as Sap and Htr (Brigatti et al., 2006).

For the respective representative models of pristine clay minerals of suitable size ($2a1b1c$), their sodium forms were proposed. The computational cell for Mnt utilized crystallographic data and the composition of Wyoming Mnt ($Na_{0.4}Ca_{0.12}[Si_{7.92}Al_{0.08}][Al_{3.08}Fe_{0.36}Mg_{0.52}]O_{20}(OH)_4$) as a reference (Tsipursky and Drits, 1984). To construct the extended computational cell with $2a1b1c$ dimensions, the original a and b cell vectors were employed. The resulting initial lattice vectors of the computational cells are presented in Table 1 for all four models of pristine smectites. In the Mnt model, two Al(III) central atoms from the octahedral sheet were replaced by two Mg(II). The summary formula of this montmorillonite model was ($Na_2[Si_{16}]$ $[Al_6Mg_2]$ $O_{32}(OH)_{24}$) (Fig. 1a).

For Bei, two Si(IV) were substituted with two Al(III) ions in the tetrahedral sheet (Fig. 1b). The octahedral sites were purely occupied by Al(III). The summary formula of the resulting $2a1b1c$ Bei model was ($Na_2[Si_{14}Al_2]$ $[Al_8]$ $O_{32}(OH)_{24}$).

Table 1. Initial lattice parameters (Å, °) and d_{001} values (Å) of pristine smectites and clay–polymer hybrids

Model	a	b	c	α	β	γ	d_{001}
Mnt	10.48	9.09	17	91.33	95.51	90.01	16.92
Mnt-PMeOx	20.97	18.18	25	91.33	95.51	90.01	24.88
Bei	10.48	9.09	17	91.33	95.51	90.01	16.92
Bei-PMeOx	20.97	18.18	25	91.33	95.51	90.01	24.88
Sap	10.48	9.07	17	90.00	97.34	90.00	16.86
Sap-PMeOx	20.74	17.85	25	90.69	90.90	90.00	25.00
Htr	10.48	9.07	17	90.00	97.34	90.00	16.86
Htr-PMeOx	20.97	18.15	25	90.00	97.34	90.00	24.80

In the case of trioctahedral saponite, the computational cell was based on the crystallographic data of talc ($Mg_3Si_4O_{10}(OH)_2$) (Drits et al., 2012). Substitutions were included, i.e. two Si(IV) were replaced with two Al(III) in the tetrahedral sheet (Fig. 1c). The chemical composition of the resulting $2a1b1c$ size of the Sap had the summary formula of $Na_2[Si_{14}Al_2]$ $[Mg_{12}]$ $O_{32}(OH)_{24}$.

Finally, also the model of Htr was built using the talc structure (Drits et al., 2012) replacing two Mg(II) ions with Li(I) in the octahedral sheet (Fig. 1d). The chemical composition of the resulting $2a1b1c$ size of the Htr model corresponded to the summary formula of $Na_2[Si_{16}]$ $[Mg_{10}$ $Li_2]$ $O_{32}(OH)_{24}$.

Due to the isomorphic substitutions in the layers, the resulting negative layer charge ($-2|e|$) in all $2a1b1c$ models was balanced by the two hydrated Na^+ within the interlayer space. These Na^+ were coordinated with four water molecules, designated as $[Na\ (H_2O)_4]^+$. The hydrated Na^+ cation was used successfully in previous work, where water molecules represented a residual water content in the Mnt samples (Moreno-Rodríguez et al., 2021).

For models of clay–polymer hybrids, the extended computational cells for clay minerals were constructed using the $4a2b1c$ framework to fit the linear pentamer unit of the neutral PMeOx polymer. To counterbalance the negative layer charge ($-6|e|$), the six hydrated Na^+ were present in the interlayer space. The presence of eight hydrated Na^+ ions in hectorite (Htr) was attributed to its higher charge density compared with other smectites (Brigatti et al., 2006). However, in $2a1b1c$ models, to maintain accuracy and minimize model size, the substitutions were consistent between Htr and other smectites. The summary of initial lattice parameters and d values of structural models of pristine clay minerals and clay–polymer hybrids are presented in Table 1.

The stability of the clay–polymer hybrid structures was examined by calculation of the intercalation energy (ΔE_{int}), according to the reaction scheme:

$$\Delta E_{int} = \sum E_{products} - \sum E_{reactants} = E(\text{CM-PMeOx}) - E(\text{CM}) - E(\text{PMeOx}), \quad (1)$$

where the CM was smectite with hydrated sodium cations: Mnt, Bei, Sap, and Htr.

PMeOx was a linear pentamer unit of the poly(2-methyl-2-oxazoline) polymer (the energy of the PMeOx molecule was computed by isolating it within the identical unit cell of the hybrid).

https://doi.org/10.1017/cmn.2024.31 Published online by Cambridge University Press

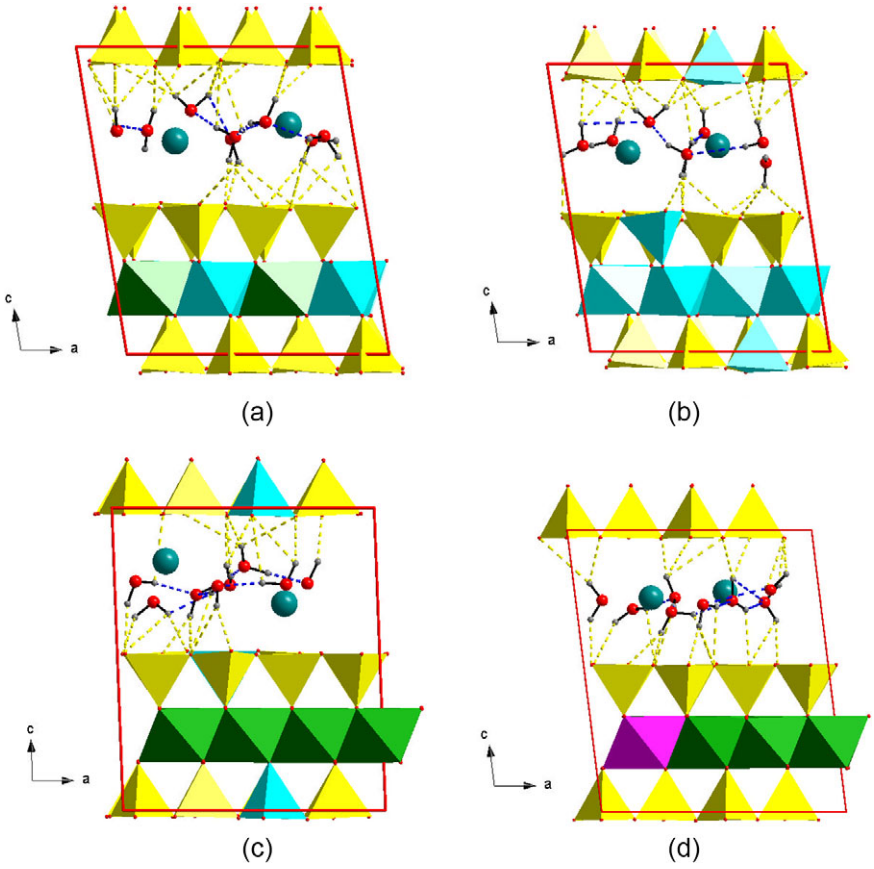

Figure 1. Optimized structural models of pristine smectite clay minerals: (a) Mnt, (b) Bei, (c) Sap, and (d) Htr. Si(IV) tetrahedra in yellow, Al(III) octahedra/tetrahedra in cyan, Mg(II) in green, and Li(I) in pink. Dashed lines for hydrogen bonds, O_w–H_w···O_w (blue) and O_w–H_w···O_b (yellow).

Results and Discussion

Structural characterization of the optimized models of smectite clay minerals

The ultimate optimized models of the pristine clay mineral system, as depicted in Fig. 1, showcased two hydrated sodium cations participating in hydrogen bond interactions with the smectite clay minerals. Following the structural optimization of the pristine clay mineral models examined, the individual molecules of hydrated sodium cations were arranged in a planar monolayer configuration within the interlayer space of the smectite clay minerals. Moreover, the basal spacing (d_{001}) was a crucial parameter reflecting the structural characterization of the clay minerals. The cell parameters and computed d_{001} values for all the optimized structural models of smectites are given in Table 2. The basal spacing of smectites is influenced by the hydration within the interlayer space, typically ranging from 10 to 18 Å depending on the hydration level of 0–3 water layers (Villar et al., 2012). The findings reported here (Table 2) confirmed that the calculated *d* values for smectites fall within this established range (Villar et al., 2012). In trioctahedral smectites (Sap and Htr), stronger interactions resulted in smaller *d* values compared with dioctahedral smectites (Mnt and Bei). The reduced basal spacings in trioctahedral smectites indicated shorter distances between repeating layers and lesser expansion of the mineral compared with dioctahedral smectites.

Table 2. Optimized lattice parameters (Å, °) and d_{001} values (Å) of pristine smectites and clay–polymer hybrids

Model	*a*	*b*	*c*	α	β	γ	d_{001}
Mnt	10.43	9.00	12.45	86.84	99.36	89.99	12.27
Mnt-PMeOx	20.79	18.00	13.87	99.36	100.18	90.09	13.47
Bei	10.34	8.87	12.57	85.17	98.56	89.96	12.38
Bei-PMeOx	20.71	17.93	14.90	93.81	100.78	90.02	14.61
Sap	10.64	9.27	12.31	85.28	92.15	89.94	12.26
Sap-PMeOx	21.30	18.48	14.26	76.77	96.52	86.97	13.78
Htr	10.56	9.16	12.28	91.96	97.02	89.94	12.18
Htr-PMeOx	21.14	18.31	14.46	92.70	104.43	90.08	13.98

Hydrogen bond analysis of pristine smectite clay minerals

The detailed analysis of hydrogen bonding interactions within the proposed 2*a*1*b*1*c* models of pristine smectites (summarized in Table 3) revealed that in each system, water molecules located in the interlayer spaces played an important role in forming relatively weak to moderate O_w–H_w···O_w and O_w–H_w···O_b hydrogen bonds. The water molecules were positioned in a planar configuration, solvating sodium cations (Fig. 1). The moderate hydrogen bonds occurred between water molecules (O_w–H_w···O_w), with a median bond length of 1.92, 1.76, 1.80, and 1.97 Å for Mnt, Bei, Sap, and

https://doi.org/10.1017/cmn.2024.31 Published online by Cambridge University Press

Table 3. D–H···A hydrogen bonds (min, median, max) (Å) in the pristine smectite clay minerals

	D–H···A			
Type of hydrogen bond	Mnt	Bei	Sap	Htr
O_w–H_w···O_w	1.75, 1.92, 2.07	1.74, 1.76, 2.95	1.73, 1.80, 1.84	1.81, 1.97, 2.87
O_w–H_w···O_b	1.84, 2.80, 2.99	1.82, 2.66, 2.96	1.88, 2.63, 2.91	1.82, 2.59, 2.88

w = water; b = basal oxygen.

Htr, respectively (Table 3). The interaction of water molecules with the clay surface was characterized by weak O_w–H_w···O_b hydrogen bonds, displaying median values of 2.80, 2.66, 2.63, and 2.59 Å for Mnt, Bei, Sap, and Htr, respectively.

Mechanical properties of pristine smectite clay minerals

Elastic constants are fundamental properties that characterize how solid materials respond to stress and strain, illustrating their capacity to withstand elastic deformation. Smectites that exhibit triclinic symmetry have 21 independent elastic constants (Gribble and Gribble, 1988). These components provide essential insights into the mechanical behavior and stability of these clay minerals under different external forces. Specifically, the elastic constants C_{11}, C_{22}, and C_{33} depict how a material compresses along different axes, while C_{44}, C_{55}, and C_{66} represent its resistance to shearing forces.

The values obtained for C_{33} were 23.84, 21.13, 24.33, and 21.30 GPa for Mnt, Bei, Sap, and Htr, respectively (Table 4). In all cases of pristine clays, C_{33} was consistently smaller than C_{22} and C_{11}, documenting that the *c* axis exhibited significantly weaker resistance to applied stress (Zhao et al., 2021). The values of C_{66} were 52.55, 54.11, 58.82, and 60.28 GPa for Mnt, Bei, Sap, and Htr, respectively. The higher values of C_{66} elastic constants compared with C_{44} and C_{55} suggested that the (001) plane had a greater resistance to the shear deformation compared with the (100) and (010) planes. These findings implied that the forces between the layers of the crystal, such as van der Waals and electrostatic forces, were much weaker compared with the binding forces between atoms within each layer (Zheng and Zaoui, 2018). Overall, all pristine smectite crystals exhibited a tendency to deform along the *c*-axis.

Furthermore, the elastic constants within the plane of the clay layer, namely C_{11}, C_{22}, C_{12}, and C_{66}, were significantly higher than those perpendicular to the basal plane, i.e. C_{33}, C_{44}, C_{55}, C_{13}, and C_{23}. This suggested that smectite layers deform more easily in the out-of-plane direction than in the in-plane direction, which reflected the strong covalent bonding within the layers. Within the category of smectites, trioctahedral smectites (Sap and Htr) exhibited higher values for C_{11}, C_{22}, and C_{33} compared with dioctahedral smectites (Mnt and Bei). This phenomenon was attributed to the heightened interaction between layers in octahedral smectites, leading to increased rigidity. Notably, Sap and Htr appeared to be more rigid than Mnt and Bei, as shown by calculated elastic parameters collected in Table 4.

The crystal's resistance to isostatic bulk compression is represented by the bulk modulus (K_{VRH}), indicating its ability to withstand compression forces. On the other hand, the shear modulus (G_{VRH}) reflects the crystal's rigidity, while Young's modulus (E_{VRH}) signifies its stiffness. Smaller values for these modulus parameters for one material compared with another suggests reduced stiffness and a heightened vulnerability to deformation under various stress conditions. Within the spectrum of smectite clay minerals, trioctahedral smectites (Sap and Htr) showcased superior mechanical properties owing to their elevated elastic moduli compared with dioctahedral smectites (Mnt and Bei). Particularly noteworthy was Htr, which stood out with greater shear modulus (G_{VRH}) and Young's modulus (E_{VRH}), while Sap exhibited a greater bulk modulus (K_{VRH}). As a result, the overall performance of Htr appeared to surpass that of the other clay minerals studied.

In contrast, Bei displayed smaller values for bulk modulus (K_{VRH}), shear modulus (G_{VRH}), and Young's modulus (E_{VRH}) in comparison with Mnt, Sap, and Htr. This observation suggested that Bei was more prone to compression, less rigid, and less stiff than the other pristine clay minerals (Mnt, Sap, and Htr, as depicted in Table 4).

For Mnt, Bei, and Sap, the calculated Poisson's ratio was 0.3, and for Htr, it was 0.2. While no prior empirical or theoretical data exist for the elastic properties of Bei, Sap, and Htr, the computed values for Mnt exhibited a strong concordance with existing literature. For instance, measurements on the elastic constants (using the weighted Hashin–Shtrikman average) of sodium-rich montmorillonite yielded values for average bulk modulus, *K*, of 35.3 GPa; average shear modulus, *G*, of 20.2 GPa; and Poisson's ratio of 0.260 (Wang et al., 1998). These measurements aligned closely with the values for Mnt calculated in the present study (Table 4), i.e. K_{VRH}=34.28 GPa, G_{VRH}=18.86 GPa, E_{VRH}=47.80 GPa, and ν=0.3.

Table 4. Calculated elastic constants C_{ij} (GPa), bulk modulus K_{VRH} (GPa), shear modulus (G_{VRH}) (GPa), Young's modulus (E_{VRH}) (GPa), and Poisson's ratio (ν) for pristine smectite clay minerals

C_{ij}	Mnt	Bei	Sap	Htr
C_{11}	142.12	130.43	141.56	160.95
C_{22}	124.04	124.27	142.37	169.71
C_{33}	23.84	21.13	24.33	21.30
C_{44}	3.59	4.64	4.38	4.55
C_{55}	–0.46	5.72	–0.44	5.45
C_{66}	52.55	54.11	58.82	60.28
C_{12}	35.97	27.08	24.36	42.32
C_{13}	1.30	2.34	2.28	–4.57
C_{23}	–3.18	2.42	0.75	–2.51
K_{VRH}	34.28	32.96	36.95	36.71
G_{VRH}	18.86	14.93	20.81	22.24
E_{VRH}	47.80	38.92	52.57	55.52
ν	0.3	0.3	0.3	0.2

https://doi.org/10.1017/cmn.2024.31 Published online by Cambridge University Press

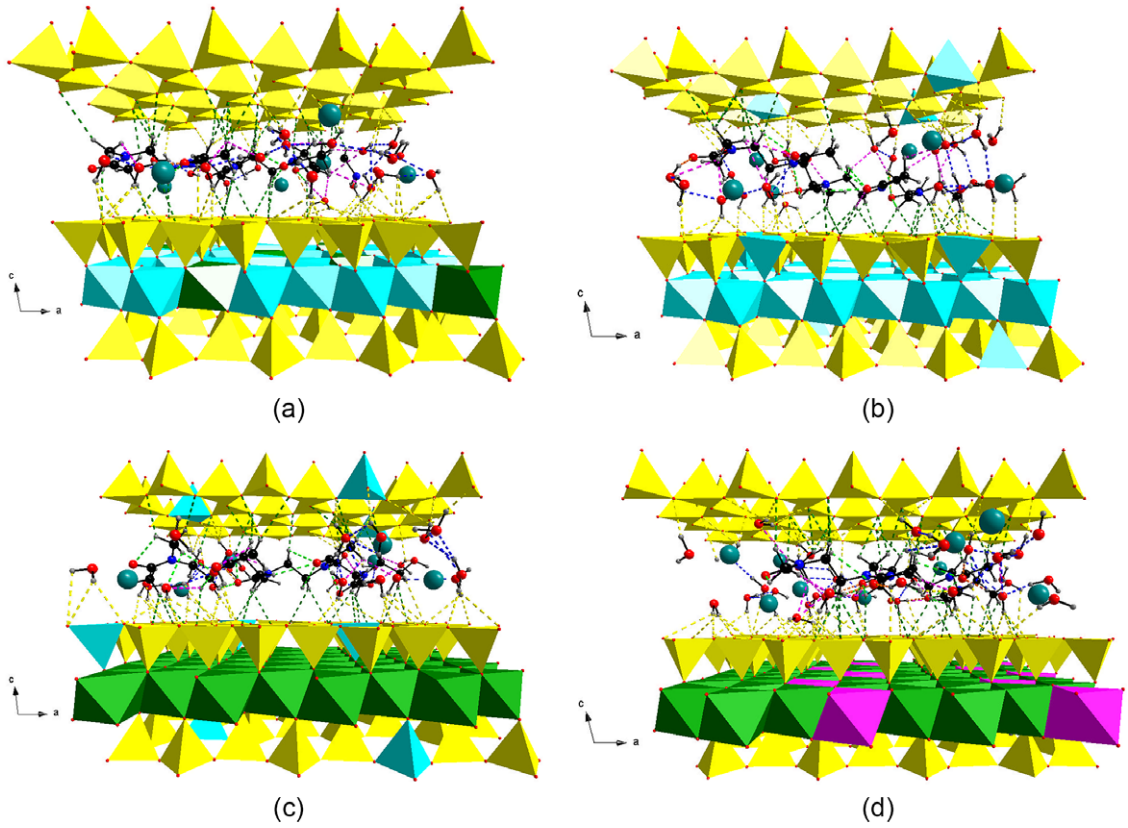

Figure 2. Hydrogen bonds in the (a) Mnt-PMeOx, (b) Bei-PMeOx, (c) Sap-PMeOx, and (d) Htr-PMeOx clay–polymer hybrid structures: C_p–H_p···O_b (green), C_p–H_p···O_w (magenta), O_w–H_w···O_w (blue), O_w–H_w···O_b (yellow), C_p–H···O_p (light green), and O_w–H_w···O_p (orange).

Structural characterization of the optimized models of clay-polymer hybrids

The structural models presented in Fig. 2 depict the fully relaxed atomic positions and cell vectors of the examined clay–polymer hybrids. The optimized d_{001} values and lattice parameters for the optimized structural models of clay–polymer hybrids are summarized in Table 2. An increase in d spacing relative to the pristine smectites indicated successful polymer intercalation into the clay–polymer hybrid systems. Hydration of and polymer intercalation into the interlayer space significantly influenced the volume expansion and resulted in expanded structures for the clay–polymer hybrids by 10, 18, 12, and 14% for Mnt-PMeOx, Bei-PMeOx, Sap-PMeOx, and Htr-PMeOx, respectively. Such relatively small expansions were due to the nearly parallel placement of the pentamer of PMeOx in the interlayer space.

Hydrogen bond analysis of clay–polymer hybrids

The comprehensive analysis of hydrogen bond interactions in the proposed models are summarized in Table 5. In each system, water molecules within the interlayer space of clay–polymer hybrids contributed to the formation of moderate to weak O_w–H_w···O_w and O_w–H_w···O_b hydrogen bonds. Similar to pristine smectite models, the strongest hydrogen bonds were observed between water molecules, with median bond lengths of 1.86, 1.90, 1.88, and 1.88 Å for Mnt-PMeOx, Bei-PMeOx, Sap-PMeOx, and Htr-PMeOx, respectively.

The examined structures further displayed C_p–H_p···O_x hydrogen bonding interactions involving the CH groups of the polymer, where O_x represents the basal oxygen atoms of the clay (O_b) and the oxygen atoms of water molecules (O_w). For Mnt-PMeOx and Htr-PMeOx, the strongest and shortest hydrogen bonds were observed in the interactions between the CH groups of the polymer and the basal oxygen atoms of the clay surface with median lengths of 2.58 and 2.77 Å, respectively. Conversely, weak hydrogen bonds occurred for C_p–H_p···O_w between the CH groups of the polymer and the oxygen atoms of water. However, in the case of Bei-PMeOx and Sap-PMeOx, the strongest and shortest hydrogen bonds were found in the interactions between the CH groups of the polymer and the oxygen atoms of water molecules with median bond lengths of 2.38 and 2.52 Å, respectively. The weakest hydrogen bond interactions were observed in C_p–H_p···O_b between the CH groups of the polymer and the basal oxygens of the saponite siloxane surface, with median hydrogen bond lengths of 2.73 and 2.67 Å, respectively (Table 5).

Structural stability of clay–polymer hybrids

The structural stability of the entire system was assessed again by estimating the intercalation energy (ΔE_{int}) according to Eqn (1). The calculated intercalation energies demonstrated that the polymer PMeOx could form a stable composite with all smectites studied, yielding ΔE_{int} values of –588, –535, –683, and –824 kJ mol^{-1} for Mnt-PMeOx, Bei-PMeOx, Sap-PMeOx, and Htr-PMeOx, respectively (Table 5). In comparison, the trioctahedral smectites (Sap and Htr) showed greater stability than the dioctahedral smectites (Mnt and Bei) because of their more rigid structure. Htr-PMeOx was the most stable of the clay–polymer hybrids investigated. These intercalation energies, which serve as an

https://doi.org/10.1017/cmn.2024.31 Published online by Cambridge University Press

Table 5. D–H···A hydrogen bonds (min, median, max) (Å) in the clay–polymer hybrids (p = polymer, w = water, b = basal oxygen), and intercalation energy (ΔE_{int}, in kJ mol^{-1})

Type of hydrogen bond	D-H···A			
	Mnt-PMeOx	Bei-PMeOx	Sap-PMeOx	Htr-PMeOx
O_w–H_w···O_w	1.71, 1.86, 2.98	1.76, 1.90, 2.99	1.74, 1.88, 2.91	1.72, 1.88, 2.92
C_p–H_p···O_w	2.29, 2.63, 2.94	2.07, 2.38, 2.91	2.35, 2.52, 2.84	2.21, 2.78, 2.91
C_p–H_p···O_b	2.30, 2.58, 2.99	2.38, 2.73, 2.96	2.28, 2.67, 2.93	2.50, 2.77, 2.95
O_w–H_w···O_b	2.07, 2.69, 2.98	1.75, 2.48, 2.99	1.75, 2.68, 2.97	1.79, 2.54, 2.99
ΔE_{int}	–588	–535	–683	–824

indicator of structural stability for the clay–polymer structures, were in full accord with the strength of the most important C_p–H_p···O_b hydrogen bonds observed in all structures. These hydrogen bonds were responsible for anchoring the polymer unit to the smectite surface. The calculated intercalation energies and the correlation with hydrogen bond strength provided strong evidence for the structural stability achieved in the clay–polymer hybrid systems.

Mechanical properties of clay–polymer hybrids

In the clay–polymer hybrids, the value of C_{33} was much smaller than that of C_{11} and C_{22}, similar to the pristine clays. This also confirmed the expected predominant deformation of the clay–polymer hybrids along the *c* axis. In addition, C_{66} was greater than C_{44} and C_{55}, which could be attributed to the greater shear resistance in the (001) plane (Table 6).

The intercalation of various molecules, including polymers, into the interlayer space of smectites is facilitated by expanding the interlayer space and weakening the forces between the layers. This resulted in a decrease in the elastic constants for the clay–polymer hybrids. For instance, the values of C_{11}, C_{22}, and C_{33} decreased in the case of clay–polymer hybrids compared with the pristine smectites. A decrease in elastic constants resulted in a decrease in the corresponding elastic moduli. For example, the value for Young's modulus (E_{VRH}) for Mnt-PMeOx decreased by 31% compared with its parent pristine clay mineral (Mnt). Similarly, the values of E_{VRH} decreased by 6, 19, and 12% for Bei-PMeOx, Sap-PMeOx, and Htr-PMeOx, respectively. Likewise, the values of bulk modulus (K_{VRH}) and shear modulus (G_{VRH}) also decreased in the case of clay–polymer hybrids. Notably, in the case of Htr-PMeOx, the bulk modulus increased as reflected by the higher value of C_{11}. These findings suggested that water and polymer in the interlayer space had a significant influence on the layer expansion in the out-of-plane direction, resulting in volume expansion and a decrease in elastic constants. In general, clay–polymer hybrids are less stiff and more elastic than their parent clays.

In a comparison of clay–polymer hybrids, a comprehensive analysis of their mechanical properties revealed a distinct prominence of Htr-PMeOx. This particular hybrid demonstrated noteworthy superiority with greater values for bulk modulus (K_{VRH}), shear modulus (G_{VRH}), and Young's modulus (E_{VRH}) compared with its counterpart clay–polymer hybrids. This heightened mechanical performance of Htr-PMeOx underscored its potential as a material with enhanced stiffness, rigidity, and resistance to compression when compared with other hybrids in the same category (Table 6). The incorporation of polymers into clay minerals has generally improved the mechanical strength of pristine polymers (Mekhzoum et al., 2020; Colombo et al., 2023; Kumari et al., 2023). Results from the present study proved that PMeOx polymer, with an indentation modulus of 8 GPa (Rettler et al., 2010), showed improved mechanical properties due to the presence of smectites as fillers with which the polymer chains formed hydrogen bonds and interacted electrostatically.

Table 6. Elastic constants (C_{ij}) (GPa), bulk modulus (K_{VRH}) (GPa), shear modulus (G_{VRH}) (GPa), Young's modulus (E_{VRH}) (GPa), and Poisson's ratio (ν) for clay–polymer hybrids

C_{ij}	Mnt-PMeOx	Bei-PMeOx	Sap-PMeOx	Htr-PMeOx
C_{11}	123.55	110.85	139.18	166.40
C_{22}	112.69	102.67	136.95	166.83
C_{33}	16.32	10.27	10.13	16.37
C_{44}	–0.17	2.42	2.86	3.02
C_{55}	2.65	1.57	2.05	4.44
C_{66}	50.18	46.37	52.29	55.28
C_{12}	26.96	23.01	31.68	57.40
C_{13}	1.69	0.93	0.27	2.75
C_{23}	0.44	0.13	1.41	2.79
K_{VRH}	28.18	22.38	26.97	37.49
G_{VRH}	12.71	14.89	17.24	19.05
E_{VRH}	33.16	36.57	42.63	48.88
ν	0.3	0.2	0.2	0.2

Conclusions

The present study investigated the effects of introducing a poly(2-methyl-2-oxazoline) polymer into smectite clay minerals (Mnt, Bei, Sap, and Htr) on their structural and mechanical properties, utilizing the density functional theory (DFT-D3) method. The mechanical properties of pristine smectite clay minerals and their hybrids by calculating elastic constants (C_{ij}) and elastic moduli (K_{VRH}, B_{VRH}, E_{VRH}) were evaluated. The poly (2-methyl-2-oxazoline) polymer interacted intensively with the smectite surfaces, resulting in the formation of Mnt-PMeOx, Bei-PMeOx, Sap-PMeOx, and Htr-PMeOx clay–polymer hybrid materials, facilitated by weak to moderate hydrogen bonding interactions (C_p–H_p···O_b).

The findings suggested that pristine smectites and their hybrids tend to undergo deformation along the *c* axis due to relatively weak

https://doi.org/10.1017/cmn.2024.31 Published online by Cambridge University Press

interlayer forces. Detailed analysis of the respective mechanical properties confirmed the assumption that clay–polymer hybrids improved mechanical properties of the pristine polymers. Moreover, such contributions by dioctahedral *vs* trioctahedral smectites were differentiated for the first time, and favored the trioctahedral smectites. After evaluating the mechanical properties of the smectites and the clay–polymer hybrids, Htr was clearly the most suitable among them for improving these properties of the PMeOX polymer. Nevertheless, the authors acknowledge that the mechanical properties of the PMeOx polymer may also be enhanced by other smectites.

Author contribution. S. Bashir - modeling, calculations, writing; D. Tunega - revising, supervising; E. Scholtzova - revising, supervising, funding, managing.

Acknowledgments. None.

Data availability statement. Data available upon request.

Financial support. Support from the Scientific Grant Agency VEGA (grants 2/0026/23 and 2/0166/21), Slovak Research and Development Agency (APVV-19-0487, APVV-22-0150), and grant Program of Slovak Academy of Sciences (SAS) for PhD students (2022-APP0426-Doktogrant) is gratefully acknowledged. The calculations were partially performed using the Vienna Scientific Cluster (VSC), project no. 70544. Some of the research results were obtained using the computational resources procured in the national project National Competence Centre for High Performance Computing (project code: 311070AKF2) funded by the European Regional Development Fund, EU Structural Funds Informatization of Society, Operational Program Integrated Infrastructure.

Competing interest. The authors declare none.

References

Adak, B., Butola, B.S., & Joshi, M. (2018). Effect of organoclay-type and clay-polyurethane interaction chemistry for tuning the morphology, gas barrier and mechanical properties of clay/polyurethane nanocomposites. *Applied Clay Science*, *161*, 343–353.

Blöchl, P.E. (1994). Projector augmented-wave method. *Physical Review B*, *50*, 17953.

Brigatti, M.F., Galan, E., & Theng, B. (2006). Structures and mineralogy of clay minerals. *Developments in Clay Science*, *1*, 19–86.

Carrier, B., Vandamme, M., Pellenq, R.J.-M., & Van Damme, H. (2014). Elastic properties of swelling clay particles at finite temperature upon hydration. *Journal of Physical Chemistry C*, *118*, 8933–8943.

Cheikh, D., Majdoub, H., & Darder, M. (2022). An overview of clay-polymer nanocomposites containing bioactive compounds for food packaging applications. *Applied Clay Science*, *216*, 106335.

Colombo, M.A., Díaz, F.R., Kodali, D., Rangari, V., Güven, O., & Moura, E.A. (2023). Influence of reinforcing efficiency of clay on the mechanical properties of poly (butylene terephthalate) nanocomposite. *Ceramics*, *6*, 58–73.

Das, P., Manna, S., Behera, A.K., Shee, M., Basak, P., & Sharma, A.K. (2022). Current synthesis and characterization techniques for clay-based polymer nano-composites and its biomedical applications: a review. *Environmental Research*, *212*, 113534.

Drits, V.A., Guggenheim, S., Zviagina, B.B., & Kogure, T. (2012). Structures of the 2:1 layers of pyrophyllite and talc. *Clays and Clay Minerals*, *60*, 574–587.

Ebrahimi, D., Pellenq, R.J.-M., & Whittle, A.J. (2012). Nanoscale elastic properties of montmorillonite upon water adsorption. *Langmuir*, *28*, 16855–16863.

Glassner, M., Vergaelen, M., & Hoogenboom, R. (2018). Poly (2-oxazoline) s: a comprehensive overview of polymer structures and their physical properties. *Polymer International*, *67*, 32–45.

Gribble, C., & Gribble, C. (1988). Physical properties of minerals. *Rutley's Elements of Mineralogy*, 26–46.

Grimme, S., Antony, J., Ehrlich, S., & Krieg, H. (2010). A consistent and accurate ab initio parametrization of density functional dispersion correction (DFT-D) for the 94 elements H-Pu. *Journal of Chemical Physics*, *132*.

Hill, R. (1952). The elastic behaviour of a crystalline aggregate. *Proceedings of the Physical Society A*, *65*, 349.

Karataş, D., Tekin, A., Bahadori, F., & Çelik, M.S. (2017). Interaction of curcumin in a drug delivery system including a composite with poly (lactic-co-glycolic acid) and montmorillonite: a density functional theory and molecular dynamics study. *Journal of Materials Chemistry B*, *5*, 8070–8082.

Karippal, J.J., Narasimha Murthy, H., Rai, K., Sreejith, M., & Krishna, M. (2011). Study of mechanical properties of epoxy/glass/nanoclay hybrid composites. *Journal of Composite Materials*, *45*, 1893–1899.

Khostavan, S., Fazli, M., Ahangari, M.G., & Rostamiyan, Y. (2019). The effect of interaction between nanofillers and epoxy on mechanical and thermal properties of nanocomposites: theoretical prediction and experimental analysis. *Advances in Polymer Technology*, *2019*, 1–10.

Kresse, G., & Furthmüller, J. (1996). Efficient iterative schemes for ab initio total-energy calculations using a plane-wave basis set. *Physical Review B*, *54*, 11169.

Kumari, N., Mohan, C., & Negi, A. (2023). An investigative study on the structural, thermal and mechanical properties of clay-based PVC polymer composite films. *Polymers*, *15*, 1922.

Le Coeur, C., Lorthioir, C., Feoktystov, A., Wu, B., Volet, G., & Amiel, C. (2021). Laponite/poly (2-methyl-2-oxazoline) hydrogels: interplay between local structure and rheological behaviour. *Journal of Colloid and Interface Science*, *582*, 149–158.

Madejová, J., Barlog, M., Slaný, M., Bashir, S., Scholtzová, E., Tunega, D., & Jankovič, Ľ. (2023). Advanced materials based on montmorillonite modified with poly (ethylenimine) and poly (2-methyl-2-oxazoline): experimental and DFT study. *Colloids and Surfaces A: Physicochemical and Engineering Aspects*, *659*, 130784.

Masood, F., ul Ain, N., Habib, S., Alam, A., Yasin, T., Hameed, A., & Farooq, M. (2022). Preparation, characterization, and evaluation of multifunctional properties of PVA/metal oxide sepiolite nanocomposite membranes for water cleanup. *Materials Today Communications*, *31*, 103620.

Mekhzoum, M.E.M., Raji, M., Rodrigue, D., & Bouhfid, R. (2020). The effect of benzothiazolium surfactant modified montmorillonite content on the properties of polyamide 6 nanocomposites. *Applied Clay Science*, *185*, 105417.

Militzer, B., Wenk, H.-R., Stackhouse, S., & Stixrude, L. (2011). First-principles calculation of the elastic moduli of sheet silicates and their application to shale anisotropy. *American Mineralogist*, *96*, 125–137.

Monjarás-Ávila, A.J., Sanchez-Olivares, G., Calderas, F., Moreno, L., Zamarripa-Calderón, J.-E., Cuevas-Suárez, C.E., & Rivera-Gonzaga, A. (2020). Sodium montmorillonite concentration effect on Bis-GMA/TEGDMA resin to prepare clay polymer nanocomposites for dental applications. *Applied Clay Science*, *196*, 105755.

Moreno-Rodríguez, D., Jankovič, Ľ., Scholtzová, E., & Tunega, D. (2021). Stability of atrazine–smectite intercalates: density functional theory and experimental study. *Minerals*, *11*, 554.

Mukhopadhyay, R., Bhaduri, D., Sarkar, B., Rusmin, R., Hou, D., Khanam, R., Sarkar, S., Biswas, J.K., Vithanage, M., & Bhatnagar, A. (2020). Clay–polymer nanocomposites: progress and challenges for use in sustainable water treatment. *Journal of Hazardous Materials*, *383*, 121125.

Nielsen, O., & Martin, R.M. (1983). First-principles calculation of stress. *Physical Review Letters*, *50*, 697.

Niu, J., Zhang, W., Li, S., Yan, W., Hao, X., Wang, Z., Wang, F., Zhang, G., & Guan, G. (2021). An electroactive montmorillonite/polyaniline nanocomposite film: superfast ion transport and ultra-affinity ion recognition for rapid and selective separation of Pb^{2+} ions. *Chemical Engineering Journal*, *413*, 127750.

Ozkose, U.U., Altinkok, C., Yilmaz, O., Alpturk, O., & Tasdelen, M.A. (2017). In-situ preparation of poly (2-ethyl-2-oxazoline)/clay nanocomposites via living cationic ring-opening polymerization. *European Polymer Journal*, *88*, 586–593.

Perdew, J.P., Burke, K., & Ernzerhof, M. (1996). Generalized gradient approximation made simple. *Physical Review Letters*, *77*, 3865.

Platen, M., Mathieu, E., Lück, S., Schubel, R., Jordan, R., & Pautot, S. (2015). Poly (2-oxazoline)-based microgel particles for neuronal cell culture. *Biomacromolecules*, *16*, 1516–1524.

https://doi.org/10.1017/cmn.2024.31 Published online by Cambridge University Press

Rettler, E.F.J., Kranenburg, J.M., Lambermont-Thijs, H.M., Hoogenboom, R., & Schubert, U.S. (2010). Thermal, mechanical, and surface properties of poly (2-N-alkyl-2-oxazoline) s. *Macromolecular Chemistry and Physics*, *211*, 2443–2448.

Sato, H., Ono, K., Johnston, C.T., & Yamagishi, A. (2005). First-principles studies on the elastic constants of a 1:1 layered kaolinite mineral. *American Mineralogist*, *90*, 1824–1826.

Scholtzová, E., & Tunega, D. (2020). Prediction of mechanical properties of grafted kaolinite – a DFT study. *Applied Clay Science*, *193*, 105692.

Scholtzová, E., Tunega, D., & Speziale, S. (2015). Mechanical properties of ettringite and thaumasite – DFT and experimental study. *Cement and Concrete Research*, *77*, 9–15.

Sharma, A., & Devi, M. (2022). A review on multiscale modelling and simulation for polymer nanocomposites. https://www.preprints.org/manuscript/202202.0213/v1

Sun, W., Wang, L., Wang, Y. (2017). Mechanical properties of rock materials with related to mineralogical characteristics and grain size through experimental investigation: a comprehensive review. *Frontiers of Structural and Civil Engineering*, *11*, 322–328.

Trachsel, L., Zenobi-Wong, M., Benetti, E.M. (2021). The role of poly (2-alkyl-2-oxazoline) s in hydrogels and biofabrication. *Biomaterials Science*, *9*, 2874–2886.

Tsipursky, S.I., & Drits, V. (1984). The distribution of octahedral cations in the 2:1 layers of dioctahedral smectites studied by oblique-texture electron diffraction. *Clay Minerals*, *19*, 177–193.

Villar, M., Gómez-Espina, R., & Gutiérrez-Nebot, L. (2012). Basal spacings of smectite in compacted bentonite. *Applied Clay Science*, *65*, 95–105.

Wang, L., Min, F., Chen, J., Zhang, L., Liu, L., & Liu, C. (2023). Flocculation performance and mechanism of P (DMDAAC-AM) on clay mineral layer: insights from DFT calculation and experiment. *Applied Surface Science*, *607*, 155089.

Wang, Y., Li, X., Qin, Y., Zhang, D., Song, Z., & Ding, S. (2021). Local electric field effect of montmorillonite in solid polymer electrolytes for lithium metal batteries. *Nano Energy*, *90*, 106490.

Wang, Z., Wang, H., & Cates, M.E. (1998). Elastic properties of solid clays, SEG Technical Program Expanded Abstracts 1998. *Society of Exploration Geophysicists*, pp. 1045–1048.

Zare, Y., Fasihi, M., & Rhee, K.Y. (2017). Efficiency of stress transfer between polymer matrix and nanoplatelets in clay/polymer nanocomposites. *Applied Clay Science*, *143*, 265–272.

Zhang, G., Wu, T., Lin, W., Tan, Y., Chen, R., Huang, Z., Yin, X., & Qu, J. (2017). Preparation of polymer/clay nanocomposites via melt intercalation under continuous elongation flow. *Composites Science and Technology*, *145*, 157–164.

Zhang, L., Min, F., Chen, J., Liu, C., & Wang, T. (2022). New insights into the interaction between monomers from acrylamide-based polymeric flocculants and montmorillonite: a DFT study. *Journal of Molecular Liquids*, *365*, 120171.

Zhao, J., Cao, Y., Wang, L., Zhang, H.-J., & He, M.-C. (2021). Investigation on atomic structure and mechanical property of Na-and Mg-Montmorillonite under high pressure by first-principles calculations. *Minerals*, *11*, 613.

Zheng, Y., & Zaoui, A. (2018). Mechanical behavior in hydrated Na-montmorillonite clay. *Physica A: Statistical Mechanics and its Applications*, *505*, 582–590.

https://doi.org/10.1017/cmn.2024.31 Published online by Cambridge University Press